RSC Advances

PAPER

View Article Online
View Journal | View Issue

Cite this: *RSC Adv.*, 2017, **7**, 49440

Improvement of NO_2 sensing characteristic for mixed potential type gas sensor based on YSZ and $Rh/Co_3V_2O_8$ sensing electrode

Jing Wang, Zhangduo Yu, Lian Wang, Bin Wang, Fangmeng Liu,* Xishuang Liang, Peng Sun, Xu Yan, Xiaohong Chuai and Geyu Lu*

Received 19th August 2017
Accepted 10th October 2017

DOI: 10.1039/c7ra09175c

rsc.li/rsc-advances

The NO_2 sensing performance of a stabilized zirconia (YSZ)-based mixed potential type gas sensor utilizing a $Co_3V_2O_8$ sensing electrode (SE) was improved by the addition of a noble metal. Among the different types of noble metal (Au, Pt, Pd and Rh), the sensor attached with $Co_3V_2O_8$-SE loaded with Rh exhibited a noticeable improvement in NO_2 response and the maximum response value was obtained when the loading mass fraction of Rh was 3 wt%. Results showed that the response for the sensor utilizing 3 wt% $Rh/Co_3V_2O_8$-SE was 113.5 mV to 50 ppm NO_2 and the sensitivity to 10–300 ppm NO_2 was 85 mV per decade at the operating temperature of 650 °C, which were enhanced by 77.5 mV and 39 mV per decade compared to those of a sensor attached with $Co_3V_2O_8$-SE, respectively. It is noteworthy that the response for each of sensor displayed a good linear relationship to the logarithm of NO_2 concentration in the ranges of 10–300 ppm at 650 °C. Additionally, the sensor attached with 3 wt% $Rh/Co_3V_2O_8$-SE also exhibited a low detection limit of 500 ppb and good selectivity to NO_2 at 650 °C. The improvement of sensing characteristics for a sensor using 3 wt% $Rh/Co_3V_2O_8$-SE may be attributed to enhanced electrochemical catalytic reaction activity to NO_2 and a mixed potential mechanism was further verified by polarization curve.

1. Introduction

Increasing NO_2 emission from automotive vehicles has caused serious environmental pollution problems, such as photochemical smog and acid rain.[1] Thus, an on-board gas sensor was urgently needed to more accurately and efficiently monitor NO_2 in the lean burn gasoline or diesel engines. The automobile exhaust gas after treatment system has the harsh conditions of high temperature, high humidity and coexistence of multiple gases. Fortunately, the solid state mixed potential type gas sensor based on stabilized zirconia (YSZ) and a metal oxide sensing electrode (SE) was capable of withstanding such a hostile environment and these have been developed and reported widely by researchers.

According to the mixed potential sensing mechanism,[2–5] the electrochemical cathodic reaction of NO_2 (1) and the electrochemical anodic reaction of oxygen (2) occured simultaneously at the triple phase boundary (TPB, SE/electrolyte/target gas) of SE and mixed potential obtained at the SE when the rates of the cathodic and anodic reactions are equal to each other. The enhanced NO_2 sensing property was related to the types of sensing electrode material. Up to now, many single and composite oxide materials[2,6–10] were developed and used for fabricating YSZ-based mixed potential type NO_2 sensor. Among the reported devices, some sensors still had room for improvement of sensing characteristics and some strategies have been performed to further enhance the sensing performance of the sensor. Lu *et al.*[11] improved the response and sensitivity of the sensor attached with In_2O_3-SE by doping different amount of MoO_3 to In_2O_3. Miura *et al.*[12,13] reported that addition of noble metal Pt to $ZnFe_2O_4$ was found to improve the sensing characteristics towards quick response and addition of Pt to In_2O_3 gave considerable improvement in selectivity. Enlightened by above strategies, the addition of small amounts of noble metal Rh to $Co_3V_2O_8$-SE was used to improve the sensing performance of mixed potential type NO_2 sensor.

Cathodic reaction:

$$NO_2 + 2e^- \rightarrow NO + O^{2-} \quad (1)$$

Anodic reaction:

$$O^{2-} \rightarrow 1/2O_2 + 2e^- \quad (2)$$

Herein, the mixed potential type sensor based on YSZ and $Co_3V_2O_8$-SE loaded with noble metals was developed to enhance the NO_2 sensing performance at high temperature. The effect of

State Key Laboratory on Integrated Optoelectronics, College of Electronic Science and Engineering, Jilin University, 2699 Qianjin Street, Changchun 130012, China. E-mail: lfm198705@126.com; lugy@jlu.edu.cn; Fax: +86-431-85167808; Tel: +86-431-85167808

types of noble metal and the amounts of Rh on the NO_2 sensing performance were investigated detailed. The reason for improvement of NO_2 sensing performance and sensing mechanism were discussed.

2. Experimental

2.1 Synthesis and characterization of sensing electrode material

The $Co_3V_2O_8$ was synthesized by a facile sol–gel method according to previous work.[14] The $Co_3V_2O_8$ loaded with different mass percentages (0 wt%, 1 wt%, 3 wt%, 5 wt% and 7 wt%) of Rh sensing electrode materials were prepared from $Co_3V_2O_8$ and stoichiometric $RhCl_3$ solution with sodium borohydride ($NaBH_4$) as the reductant. The $Co_3V_2O_8$ loaded with other types of noble metal (Au, Pt and Pd) sensing materials were prepared with the same method according to above-described procedure, respectively.

X-ray diffraction (XRD) patterns of sensing electrode materials obtained were characterized by Rigaku wide-angle X-ray diffractometer (D/max rA, using Cu Kα radiation at wave length = 0.1541 nm) in the angular range of 10–80°. Field-emission scanning electron microscopy (FESEM) observations of surface morphology of sensing electrodes were measured using a JEOL JSM-6500F microscope with an accelerating voltage of 15 kV. X-ray photoelectron spectroscopy (XPS) measurements were performed on a Thermo ESCALAB250 spectrometer equipped with an Al-Kα ray source.

2.2 Fabrication and measurement of gas sensor

As previously reported procedure,[15] the sensors were fabricated using YSZ plate (8 mol% Y_2O_3-doped, 2 mm × 2 mm square, 0.3 mm thickness, provided by Anpeisheng Corp., China) and the $Co_3V_2O_8$-SE loaded with different types of noble metal or different weight percentages of Rh, respectively. The sensors attached with $Co_3V_2O_8$-SE loaded with 0 wt%, 1 wt%, 3 wt%, 5 wt% and 7 wt% Rh were labeled as S0, S1, S3, S5 and S7, respectively and the schematic diagram of developed sensor was showed in Fig. 1. The gas sensing performances of the fabricated sensors were measured by a conventional static method.[16,17] The current–voltage (polarization) curves of sensors were carried out according to the potentiodynamic method (CHI600C, Instrument corporation of Shanghai, China) using a two-electrode configuration in air and NO_2 gas at 650 °C.

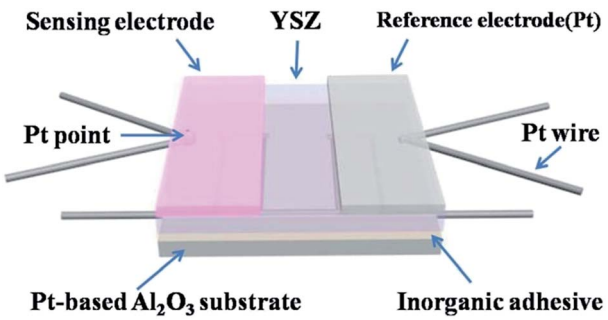

Fig. 1 Schematic diagram of developed sensor.

3. Results and discussion

Fig. 2 displays XRD patterns of $Co_3V_2O_8$ and 3 wt% Rh/$Co_3V_2O_8$ sensing electrode materials. All diffraction peaks of $Co_3V_2O_8$ were readily indexed to orthorhombic structure of $Co_3V_2O_8$ composite oxide, which agreed well with the standard XRD card (JCPDS#74-1486). No impurity phases were observed in the pattern, which suggests the high purity of material. However, no obvious Rh-related diffraction peaks were found in the XRD pattern of 3 wt% Rh/$Co_3V_2O_8$ sensing material, which maybe due to the small amount of Rh or the incomplete crystallinity induced by lower sintering temperature of sensing material.

The surface morphology of 3 wt% Rh/$Co_3V_2O_8$ sensing electrode was characterized by FESEM and the corresponding result is shown in Fig. 3(a). It can be clearly seen that the sensing material was composed of micron-scale particle and porous structure, which was contributed to diffusion of the gas molecular within the sensing electrode layer. The EDS mapping image of 3 wt% Rh/$Co_3V_2O_8$ sensing electrode was measured and used to observe the existence and distribution of Rh element, as exhibited in Fig. 3(b). Obviously, the EDS mapping measurement of 3 wt% Rh/$Co_3V_2O_8$ sensing electrode confirmed the existence and homogeneous distribution of Rh element.

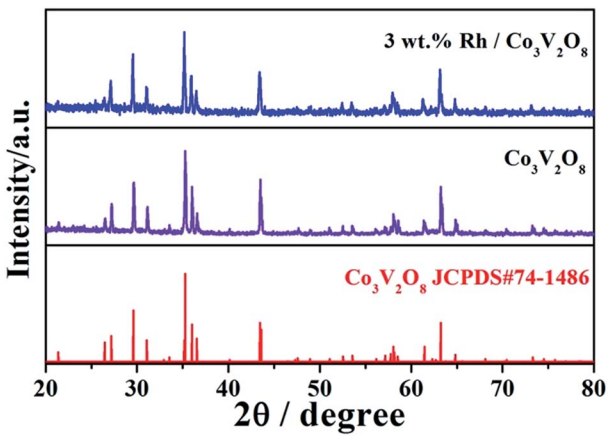

Fig. 2 XRD patterns of $Co_3V_2O_8$ and 3 wt% Rh/$Co_3V_2O_8$ sensing electrode materials.

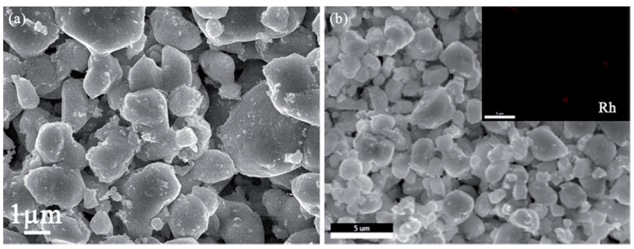

Fig. 3 (a) SEM image of 3 wt% Rh/$Co_3V_2O_8$ sensing electrode; (b) EDS mapping image of 3 wt% Rh/$Co_3V_2O_8$.

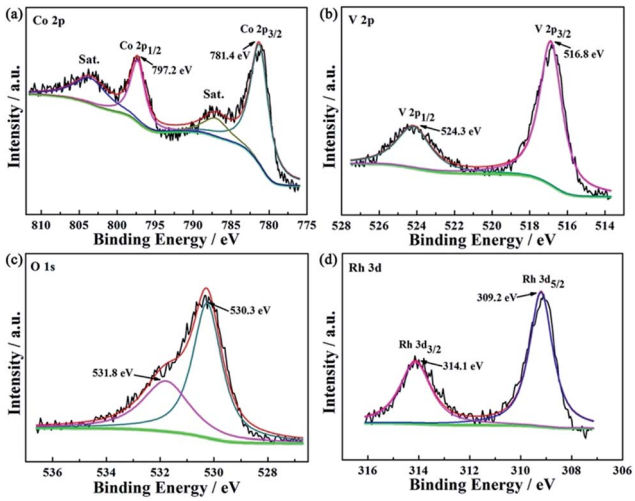

Fig. 4 XPS spectra of 3 wt% Rh/$Co_3V_2O_8$ sensing electrode material (a) Co 2p; (b) V 2p; (c) O 1s and (d) Rh 3d.

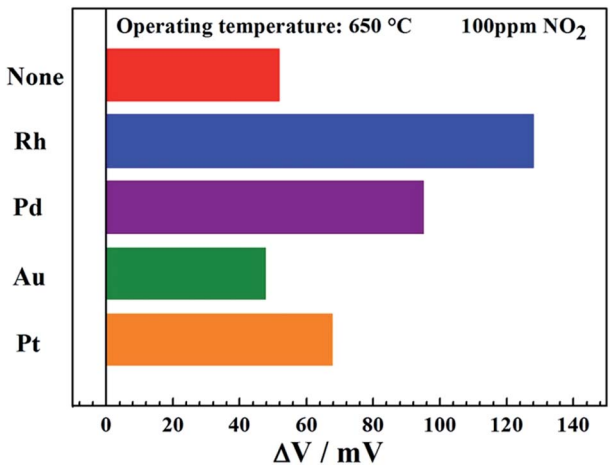

Fig. 5 Response values of sensors attached with $Co_3V_2O_8$-SE loaded with different types of noble metals to 100 ppm NO_2 at 650 °C.

To further determinate the surface compositions and chemical states of the prepared 3 wt% Rh/$Co_3V_2O_8$ sensing material, XPS measurement was performed. Fig. 4(a) shows the high resolution Co 2p spectrum of sensing material. The binding energy peak positions at around 797.2 and 781.4 eV could be assigned to Co $2p_{1/2}$ and Co $2p_{3/2}$. And the binding energy width equal to 15.8 eV between the main signals of the Co $2p_{1/2}$ and Co $2p_{3/2}$ doublet corresponded to Co^{2+}.[18–20] Moreover, the spectrum peak displayed satellites at each of high-energy sides, which could be traced back to the shake-up process.[21] Such signals further confirmed the presence of Co^{2+} at the surface of 3 wt% Rh/$Co_3V_2O_8$.[22] In Fig. 4(b), the spectrum can be deconvoluted to two distinct diffraction peaks at 524.3 and 516.8 eV, which could be related to V $2p_{1/2}$ and V $2p_{3/2}$, respectively.[23] The binding energy width of V 2p was equal to 7.5 eV, which can be confirmed V^{5+} valence state.[24] Additionally, the O 1s spectrum was asymmetric and could be fitted into two peaks (Fig. 4(c)). The binding energy peaks positioned at around

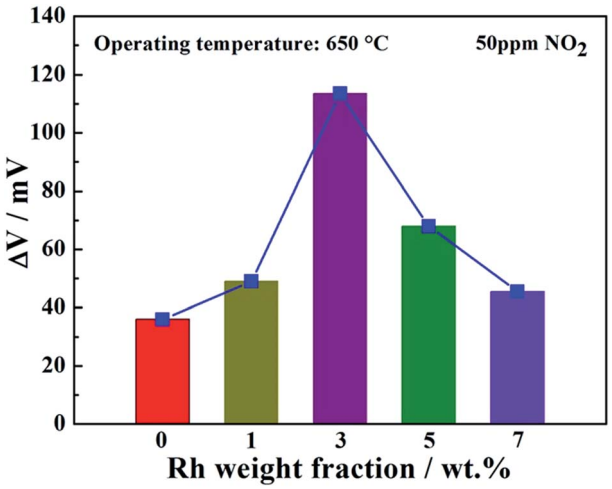

Fig. 6 Responses of the sensor attached with $Co_3V_2O_8$-SE loaded with different weight fractions of Rh to 50 ppm NO_2 at 650 °C.

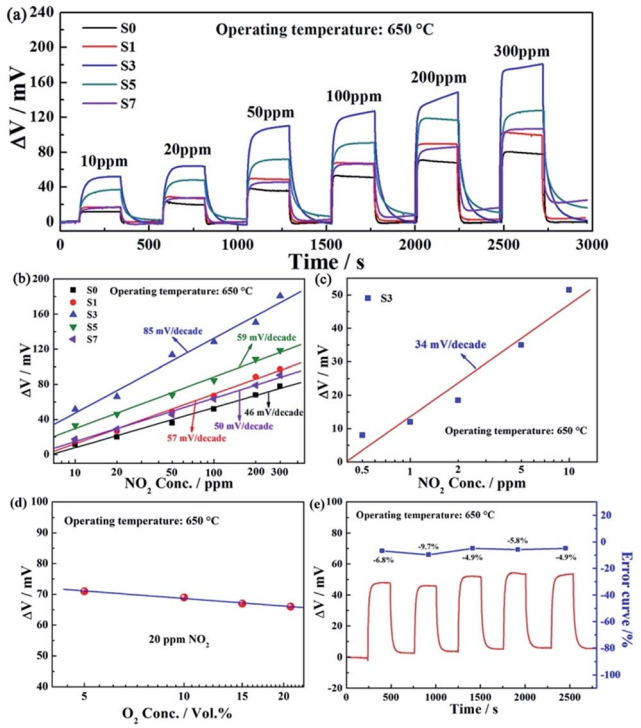

Fig. 7 (a) Response transients for sensors S0–S7 toward different concentrations of NO_2 in the range of 10–300 ppm at 650 °C; (b) dependence of ΔV on the logarithm of NO_2 concentrations for sensors S0–S7 at 650 °C; (c) dependence of ΔV for sensor S3 on the logarithm of NO_2 concentrations in the range of 0.5–10 ppm at 650 °C; (d) dependence of ΔV for the sensor S3 to 20 ppm NO_2 on the logarithm of O_2 concentrations; (e) continuous response and recovery transients of the sensor S3 to 10 ppm NO_2 at 650 °C.

531.8 and 530.3 eV were attributed to oxygen species related to the adsorbed water molecules (H_2O_{ads}) and typical lattice oxygen in the surface of $Co_3V_2O_8$ sensing material, respectively.[25] The Rh-related binding energy peak in 3 wt% Rh/$Co_3V_2O_8$ sensing material was also observed and diffraction

peaks located at 309.2 and 314.1 eV were assigned to Rh $3d_{5/2}$ and Rh $3d_{3/2}$ of Rh^{3+}, respectively, rather than the metal phase Rh^0 (ref. 26 and 27) (Fig. 4(d)).

The response values of sensors attached with $Co_3V_2O_8$-SE loaded with different types of noble metals (Rh, Pd, Au and Pt) to 100 ppm NO_2 at 650 °C were measured and demonstrated in Fig. 5. Apparently, the sensor utilizing $Co_3V_2O_8$-SE loaded with Rh displayed the highest response value to 100 ppm NO_2 at 650 °C, compared with the devices attached with $Co_3V_2O_8$-SE loaded with other noble metals. Therefore, the detailed sensing characteristics of the sensor using $Co_3V_2O_8$-SE loaded with Rh were paid considerable attentions to investigate in the next work. In order to study the effect of different weight fractions of Rh in $Co_3V_2O_8$-SE on NO_2 sensing property and determinate the optimal Rh loading amount, the response of the sensor attached with $Co_3V_2O_8$-SE loaded with different weight fractions of Rh to 50 ppm NO_2 at 650 °C was investigated and depicted in Fig. 6. It can be clearly observed that the response value of the sensor exhibited a "peak" shape with a trend of "increase-maximum-decrease" to 50 ppm NO_2 with the increase of loading weight fraction of Rh in the range of 0–7 wt% and the highest response value was obtained when the loading weight fraction of Rh was 3 wt%.

Fig. 7(a) shows the response transients for sensors S0–S7 toward different concentrations of NO_2 in the range of 10–300 ppm at 650 °C. The responses of the sensor S3 to every concentrations of NO_2 in the range of 10–300 ppm were higher than those of sensor S0, S1, S5 and S7. The response value of the sensor S3 to 50 ppm NO_2 was 113.5 mV at 650 °C, which was approximately 3.15, 2.32, 1.67 and 2.50 times higher than those of sensor S0, S1, S5 and S7, respectively. The dependence of ΔV on the logarithm of NO_2 concentrations for sensors S0–S7 at 650 °C is displayed in Fig. 7(b). It was revealed that ΔV for the sensors S0–S7 and the logarithm of NO_2 concentration in the range of 10–300 ppm at 650 °C almost showed a linear relationship, which conformed to the mixed potential type model.[5,10] The sensitivity of the sensor S3 to 10–300 ppm NO_2 was 85 mV per decade, which was 39 mV per decade higher than that of sensor S0. The comparison of NO_2 sensing performances for the sensor S3 and those reported previously in literature is listed in Table 1. Obviously, the sensors S3 exhibited better sensing properties to NO_2 comparing with other devices. Additionally, as indicated in Fig. 7(c), it is surprising that the sensor S3 displayed the low detection limit of 0.5 ppm and the response value of present sensor almost varied linearly with the logarithm of NO_2 concentration in the range of 0.5–10 ppm, which the sensitivity was as large as 34 mV per decade. Furthermore, the effect of different oxygen concentrations on sensing characteristic is evaluated and the corresponding results are demonstrated in Fig. 7(d). Obviously, the response of the fabricated sensor S3 increased slightly with the decreasing of oxygen partial pressure and ΔV varied linearly with the logarithm of O_2 concentrations in the range of 5–21 vol% at 650 °C. Moreover, the continuous response and recovery characteristic for the present sensor is also an important sensing performance parameter. The continuous response and recovery transients of the fabricated sensor S3 to 10 ppm NO_2 at 650 °C, as illustrated in Fig. 7(e). It is clearly seen that the responses of the present device to 10 ppm NO_2 had little fluctuation and the best change error was −9.7% in the examined five-time cycles, which indicated that the sensor displayed comparatively good repeatability.

Table 1 Comparison of the sensing performance of the present sensor and those of devices reported in literatures

Material	Operating temperature (°C)	NO_2 conc. (ppm)	Response (mV)	Sensitivity (mV per decade)	Ref.
Rh–$Co_3V_2O_8$	650	100	128.5	85	This work
NiO	850	400	75	—	2
WO_3	600	200	65	—	6
ZnO	700	50	40	—	7
$Ni_{0.95}Cr_{0.03}O_{1-\delta}$	800	200	50	—	28
Rh–NiO	800	50	77	—	29
Cr_2O_3–WO_3	800	100	51.6	25	30
NiO–CuO	800	400	28	—	31
$SmFeO_3$	500	90	64	—	8
$La_{0.65}Sr_{0.35}MnO_3$	500	100	50	36.6	32
$(La_{0.8}Sr_{0.2})_2$-$FeNiO_{6-\delta}$	550	200	53.7	71.8	3
$ZnFe_2O_4$	700	200	41	24	33
$MnCr_2O_4$	650	100	73	44.5	9
$CdCr_2O_4$	500	200	65	40	34
$Bi_2W_2O_9$	500	200	53	54.8	35
$CoNb_2O_6$	750	100	99	52	10
$CoTa_2O_6$	650	100	93	80	36

The selectivity of the sensor, as an important evaluation criterion for sensing characteristics, was investigated. The response values of the sensor S3 to 50 ppm of various gases, such as NO_2, H_2, NO, NH_3, CO, CH_4 and C_2H_4 were measured at 650 °C, as shown in Fig. 8. It revealed that the sensor S3 exhibited the highest response value toward 50 ppm NO_2 as oppose to other interfering gases, which indicated that the present sensor displayed the excellent selectivity to NO_2 at 650 °C.

In order to more clearly elucidate the degree of electrochemical reaction at TPB for sensor S0 and S3 and to further explain the reason for improvement of NO_2 sensing performance by loading Rh in $Co_3V_2O_8$-SE, the polarization curves of the sensor S0 and S3

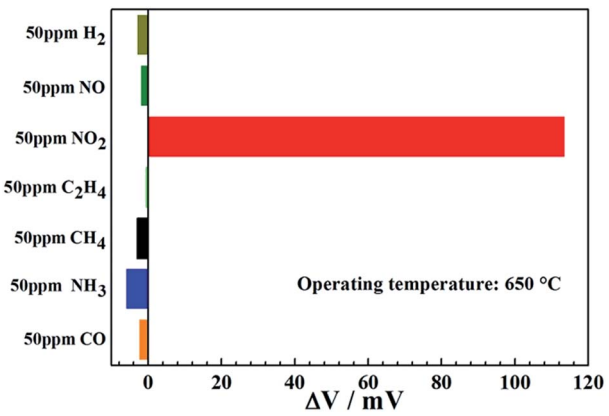

Fig. 8 Selectivity of the sensor S3 to various gases at 650 °C.

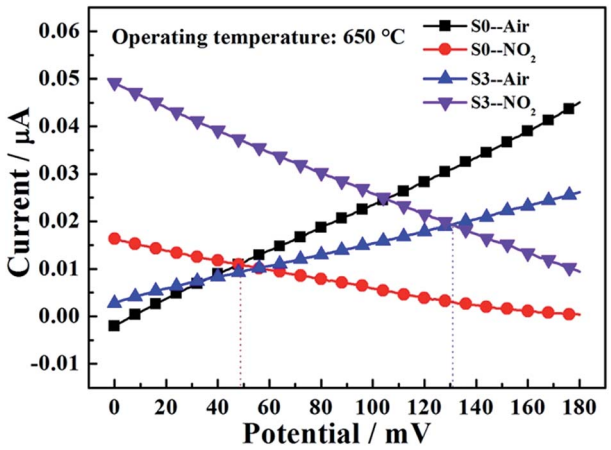

Fig. 9 Polarization curves for the sensor S0 and S3 in air and 100 ppm NO_2 at 650 °C.

Table 2 Comparison of the mixed potential estimated and the potential difference value observed for the sensor S0 and S3

Sensors	NO_2 conc. (ppm)	Mixed potential (estimated) (mV)	Potential difference value (observed) (mV)
S0	100	49	52
S3	100	131	128.5

in air and sample gas (100 ppm NO_2 + air) at 650 °C were measured, as shown in Fig. 9. From the perspective of a mixed-potential model,[5,6,15] higher NO_2 sensitivity can be achieved by one or combination of the following conditions: an increase in the polarization curve to cathodic reaction of NO_2 and a decrease in the polarization curve to anodic reaction of O_2. Clearly, for the sensor S3, the polarization curve for anodic reaction of O_2 decreased slightly and the polarization curve for cathodic reaction of NO_2 shifted significantly upward, compared with those of the sensor S0. The above result demonstrated that the electrochemical catalytic reaction activity to NO_2 was enhanced obviously and the electrochemical catalytic activity to anodic reaction of O_2 was lowered marginally when the Rh was loaded into $Co_3V_2O_8$-SE. Therefore, the improvement of NO_2 sensing performance was mainly attributed to the enhanced electrochemical catalytic reaction activity to NO_2 because of addition of Rh. Additionally, the mixed potential can be estimated from the intersection of the cathodic and anodic polarization curves. Based on the comparison of the mixed potential estimated values and the potential difference values experimentally observed in Table 2. The mixed potential values (49 and 131 mV) for sensor S0 and S3 to 100 ppm NO_2 are close agreement with the potential difference values (52 and 128.5 mV), indicating that the sensing mechanism of developed sensor abided by the mixed-potential model.

4. Conclusions

The stabilized zirconia-based mixed potential type NO_2 sensor utilizing $Co_3V_2O_8$-SE loaded with different types of noble metal were fabricated and developed to improve the sensing characteristics at elevated temperature. Among the loading noble metals (Rh, Au, Pt and Pd), Rh was found to give the largest enhancement in NO_2 response value. The gas sensing test results showed that the sensor attached with $Co_3V_2O_8$-SE loaded with 3 wt% Rh displayed the highest response of 113.5 mV to 50 ppm NO_2 and sensitivity of 85 mV per decade to 10–300 ppm NO_2 at 650 °C. Interestingly, the present device also exhibited the low detection limit of 500 ppb and excellent selectivity to NO_2 at 650 °C. Based on polarization curves measurement results, the mixed potential mechanism was verified and the improvement of NO_2 sensing characteristics was speculated to be assigned to enhanced electrochemical catalytic reaction activity to NO_2.

Conflicts of interest

There are no conflicts to declare.

Acknowledgements

This work is supported by the National Nature Science Foundation of China (No. 61327804, 61520106003, 61374218, 61533021, 61474057, 61473132 and 61503148), Program for Chang Jiang Scholars and Innovative Research Team in University (No. IRT13018) and National High-Tech Research and Development Program of China (863 Program, No. 2014AA06A505), National Key Research and Development Program of China (No. 2016YFC0207300 and 2016YFC0201002), Application and Basic Research of Jilin Province (2013010 2010JC).

Notes and references

1 R. Moos, B. Reetmeyer, A. Hürland and C. Plog, *Sens. Actuators, B*, 2006, **119**, 57–63.
2 N. Miura, J. Wang, M. Nakatou, P. Elumalai, S. Zhuiykov and M. Hasei, *Sens. Actuators, B*, 2006, **114**, 903–909.
3 L. Zhou, X. Li, H. Wu, Z. Liao, Q. Yuan, F. Xia and J. Xiao, *Ceram. Int.*, 2014, **40**, 9257–9263.
4 G. Lu, Q. Diao, C. Yin, S. Yang, Y. Guan, X. Cheng and X. Liang, *Solid State Ionics*, 2014, **262**, 292–297.
5 N. Miura, T. Sato, S. Anggraini, H. Ikeda and S. Zhuiykov, *Ionics*, 2014, **20**, 901–925.
6 G. Lu, N. Miura and N. Yamazoe, *Sens. Actuators, B*, 2000, **65**, 125–127.
7 N. Miura, K. Akisada, J. Wang, S. Zhuiykov and T. Ono, *Ionics*, 2004, **10**, 1–9.
8 H. Giang, H. Duy, P. Ngan, G. Thai, D. Thu, D. Thu and N. Toan, *Sens. Actuators, B*, 2013, **183**, 550–555.
9 Q. Diao, C. Yin, Y. Guan, X. Liang, S. Wang, Y. Liu, Y. Hu, H. Chen and G. Lu, *Sens. Actuators, B*, 2013, **177**, 397–403.
10 F. Liu, B. Wang, X. Yang, Y. Guan, R. Sun, Q. Wang, X. Liang, P. Sun and G. Lu, *Sens. Actuators, B*, 2016, **232**, 523–530.
11 H. Cai, R. Sun, X. Yang, X. Liang, C. Wang, P. Sun, F. Liu, C. Zhao, Y. Sun and G. Lu, *Ceram. Int.*, 2016, **42**, 12503–12507.
12 S. Zhuiykov, T. Ono, N. Yamazoe and N. Miura, *Solid State Ionics*, 2002, **152–153**, 801–807.

13 R. Wama, V. Plashnitsa, P. Elumalai, T. Kawaguchi, Y. Fujio, M. Utiyama and N. Miura, *J. Electrochem. Soc.*, 2009, **156**, J102–J107.
14 F. Liu, Y. Guan, M. Dai, H. Zhang, Y. Guan, R. Sun, X. Liang, P. Sun, F. Liu and G. Lu, *Sens. Actuators, B*, 2015, **216**, 121–127.
15 F. Liu, Y. Guan, H. Sun, X. Xu, R. Sun, X. Liang, P. Sun, Y. Gao and G. Lu, *Sens. Actuators, B*, 2015, **222**, 698–706.
16 B. Wang, F. Liu, X. Yang, Y. Guan, C. Ma, X. Hao, X. Liang, F. Liu, P. Sun, T. Zhang and G. Lu, *ACS Appl. Mater. Interfaces*, 2016, **8**, 16752–16760.
17 C. Wang, X. Cheng, X. Zhou, P. Sun, X. Hu, K. Shimanoe, G. Lu and N. Yamazoe, *ACS Appl. Mater. Interfaces*, 2014, **6**, 12031–12037.
18 W. Chu, P. Chernavskii, L. Gengembre, G. Pankina, P. Fongarland and A. Khodakov, *J. Catal.*, 2007, **252**, 215–230.
19 W. Ni, S. Liu, Y. Fei, Y. He, X. Ma, L. Lu and Y. Deng, *J. Mater. Chem. A*, 2016, **4**, 7746–7753.
20 Z. Liu, J. Hao, L. Fu and T. Zhu, *Appl. Catal., B*, 2003, **44**, 355–370.
21 M. Voß, D. Borgmann and G. Wedler, *J. Catal.*, 2002, **212**, 10–21.
22 C. Jia, M. Schwickardi, C. Weidenthaler, W. Schmidt, S. Korhonen, B. Weckhuysen and F. Schüth, *J. Am. Chem. Soc.*, 2011, **133**, 11279–11288.
23 Z. Qin, J. Pei, G. Chen, D. Chen, Y. Hu, C. Lv and C. Bie, *New J. Chem.*, 2017, **41**, 5974–5980.
24 V. Soundharrajan, B. Sambandam, J. Song, S. Kim, J. Jo, P. Duong, S. Kim, V. Mathew and J. Kim, *J. Colloid Interface Sci.*, 2017, **501**, 133–141.
25 J. Zhang, B. Yuan, S. Cui, N. Zhang, J. Wei, X. Wang, D. Zhang, R. Zhang and Q. Huo, *Dalton Trans.*, 2017, **46**, 3295–3302.
26 N. Kim, S. Choi, S. Kim, H. Cho, J. Jang, W. Koo, M. Kim and I. Kim, *Sens. Actuators, B*, 2016, **224**, 185–192.
27 K. Choi, S. Hwang, Z. Dai, Y. Kang and J. Lee, *RSC Adv.*, 2014, **4**, 53130–53136.
28 P. Elumalai, J. Zosel and U. Guth, *Ionics*, 2009, **15**, 405–411.
29 J. Wang, P. Elumalai, D. Terada, M. Hasei and N. Miura, *Solid State Ionics*, 2006, **177**, 2305–2311.
30 Q. Diao, C. Yin, Y. Liu, J. Li, X. Gong, X. Liang, S. Yang, H. Chen and G. Lu, *Sens. Actuators, B*, 2013, **180**, 90–95.
31 V. Plashnitsa, T. Ueda and N. Miura, *Int. J. Appl. Ceram. Technol.*, 2006, **3**, 127–133.
32 L. Wu, J. Xia, W. Shi, D. Jiang and Q. Li, *Ionics*, 2016, **22**, 927–934.
33 N. Miura, S. Zhuiykov, T. Ono, M. Hasei and N. Yamazoe, *Sens. Actuators, B*, 2002, **83**, 222–229.
34 G. Lu, N. Miura and N. Yamazoe, *J. Mater. Chem.*, 1997, **7**, 1445–1449.
35 L. Wu, J. Xia, J. Wu and Q. Li, *Ionics*, 2015, **21**, 3239–3244.
36 F. Liu, B. Wang, X. Yang, Y. Guan, Q. Wang, X. Liang, P. Sun, Y. Wang and G. Lu, *Sens. Actuators, B*, 2017, **240**, 148–157.